Minireview

Proton conduction through the M2 protein of the *influenza A* virus; a quantitative, mechanistic analysis of experimental data

James D. Lear*

Johnson Research Foundation, Department of Biochemistry and Biophysics, School of Medicine of the University of Pennsylvania, Philadelphia, PA 19104-6059, USA

Received 19 March 2003; revised 13 May 2003; accepted 13 May 2003

First published online 17 July 2003

Edited by Maurice Montal

Abstract The M2 proton channel from *influenza A* virus forms proton-selective ion channels, which are the target of the drug amantadine. Here, existing experimental data are quantitatively examined for insights into mechanisms to account for the pH- and voltage-dependences of M2 proton conduction. The analysis shows that a model involving protonation equilibria of His^{37}, including pH-dependent changes in the relative rates of diffusion on either side of the pore, is quantitatively able to account for recently reported electrophysiological data examining the pH- and voltage-dependences of Rostock and Weybridge strain M2 proton conduction.

Key words: Influenza M2; Viral matrix protein; Proton channel; Conduction mechanism

1. Introduction

Proton conductance is as important to biology as electron transport [1]. Unlike electrons, which appear to traverse protein structures independently of the protein's composition [2], protons require a continuous chain of rotationally mobile proton acceptors, usually water molecules [3–5]. The M2 channel from *influenza A* virus, a 97-residue protein that forms highly selective proton channels [6], offers an opportunity to examine proton conductance in a membrane protein of defined sequence for which plausible structural models have been made [7–18]. The active form of the channel has been demonstrated to be a tetramer [19]. The four monomers have a single transmembrane helix, with a His residue (His^{37}) that is essential for the proton selectivity of M2 [20,21]. Structural models all show a water-filled pore interrupted at only one position, His^{37}. The proton channel activity of most strains is inhibited by the drug amantadine, although resistant strains with mutations within the M2 transmembrane helix have been isolated [7,22–24]. Amantadine may be considered as a hydrophobically stabilized proton surrogate that competes directly with protons for binding to the electron lone pairs of His^{37} [25]. A similar, strong inhibitory effect of Cu^{2+} ions supports this interpretation [21].

From many different electrophysiological studies of heterologously expressed M2 [20,21,23,26–32], the qualitatively defining properties of the channel, all of which depend on the presence of the His^{37} residue, are:

1. Essentially perfect selectivity for protons [26,27,30,33].
2. A sigmoidal increase of inward current with lower external pH [26,27,29].
3. Less current with $pH_{in} < pH_{out}$ versus $pH_{out} < pH_{in}$ [27,34].
4. Concentration-, pH-, and voltage-dependent reduction of proton currents by amantidine and rimantidine [26,30,35].
5. Very small ($<$ fS; 1 fS $= 10^{-15}$ Ω^{-1}) unitary conductance [28,33].

All proposed structural models are in good agreement with respect to the identities of the side chains lining the pore. There are, however, significant differences in proposed conduction mechanisms. In one, [7], an ε-protonated histidine residue accepts a second, extra-cellular proton on its δ nitrogen, then releases the ε-proton into the intracellular environment. Subsequent tautomerization restores the histidine to its initial, singly protonated state, ready to repeat the process. Indirect support for this was provided by molecular dynamics studies [36] and from the observation that proton flux was more severely reduced in D_2O buffers than would be expected from the viscosity increase alone, indicating that H_3O^+ was not the actively diffusing species [28]. In another, quite different mechanism [10,12,37], successive protonation of the four available histidine residues in the tetramer moves the His residues apart due to electrostatic repulsion. Much as with opening a faucet, this would increase the rate of water and proton flux across the membrane. Molecular dynamics simulations [9] suggest that the doubly protonated tetramer has a more open structure than the singly protonated one, again implying a higher intrinsic conductivity. Recently [38], a molecular dynamics study specifically formulated to consider proton transfers was performed on a model of the M2 transmembrane tetramer with four ε-protonated histidines along with an extra proton. No histidine ε-proton dissociation was considered in this simulation, which gave computed proton diffusion constants near to those of bulk water and predicted proton passage times on the order of a nanosecond or less as long as side-chain mobility was allowed.

To distinguish among different mechanisms, it is necessary to consider their quantitative implications. Previously [25], a very elementary 'state transition' model (cf. e.g. [39]) was de-

*Fax: (1)-215-898 4217.
E-mail address: lear@mail.med.upenn.edu (J.D. Lear).

Abbreviations: Standard one- or three-letter codes for amino acid residues (e.g. H, His = histidine); $[H^+]$, proton concentration in mol/l

0014-5793/03/$22.00 © 2003 Published by Elsevier B.V. on behalf of the Federation of European Biochemical Societies.
doi:10.1016/S0014-5793(03)00778-6

veloped by considering the rates of intra- and extra-cellular proton exchange of three different histidine states in the tetramer (His, His·H^+, and $His_2 \cdot H_2^+$). With the rate constants defined as functions of transmembrane voltage, models such as this can predict the proton current as a function of solution pH, voltage, and the pK_a of the different histidine protonation states. The model was, in fact, successfully applied to quantitatively account for published data [26], showing a sigmoidal pH dependence of M2 chord conductance on external solution pH. Here, this mechanism has been extended to include the possibility of a third His protonation state ($His_3 \cdot H_3^+$), and generalized to allow for somewhat more complex electrostatic effects on rate constants than afforded by fixed barrier and site positions. The mechanism, tested against an extensive set of recently published current–voltage and current–pH data obtained from M2 expressed in mouse erythroleukemia (MEL) cells [27] is able to account well for proton conduction over the observed range of voltages at three different pH gradients. However, in order to do this, the mechanism requires either significant voltage-dependent changes in site electrical distance parameters or a pH-dependent change in the ratio of proton diffusion constants on the two sides of the pore.

2. Methods

A three-site mechanism for proton conductance in the influenza virus M2 channel was derived from the equilibrium scheme:

$$H^+_{out} + S_0 \underset{k_{0b}}{\overset{k_{0f}}{\leftrightarrow}} S_1 \underset{k_{1b}}{\overset{k_{1f}}{\leftrightarrow}} H^+_{in} + S_0$$

$$H^+_{out} + S_1 \underset{k_{2b}}{\overset{k_{2f}}{\leftrightarrow}} S_2 \underset{k_{3b}}{\overset{k_{1f}}{\leftrightarrow}} H^+_{in} + S_1$$

$$H^+_{out} + S_2 \underset{k_{4b}}{\overset{k_{4f}}{\leftrightarrow}} S_3 \underset{k_{5b}}{\overset{k_{5f}}{\leftrightarrow}} H^+_{in} + S_2$$

where H^+_{out} and H^+_{in} are proton concentrations outside and inside, S_0, S_1, S_2, and S_3 represent the fractions of total channel site concentration in, respectively, non-, singly-, doubly-, and triply-protonated forms. The ks are rate constants for the forward and backward reactions as written.

The current i, defined using electrophysiological conventions as the net rate of proton transport per unit site from 'in' to 'out', can be calculated as a function of the site and hydrogen ion concentrations from the mass action rate equations using the assumption of a steady-state concentration of all sites. After some lengthy, but straightforward algebra the equation for current (in units of hydrogen ion concentration per site per unit time) is[1]:

$$i = f^* + [a^* - f^*]bdf/A + [b^* + c^* - f^*]adf/A + [d^*e^* - f^*]acf/A \quad (1)$$

where the constants are linear combinations of specific rates defined by:

$$a \equiv k_{0f}H^+_{out} + k_{1b}H^+_{in};\ a^* \equiv -k_{0f}H^+_{out} + k_{1b}H^+_{in}$$

$$b \equiv k_{0b} + k_{1f};\ b^* \equiv k_{0b} - k_{1f}$$

$$c \equiv k_{2f}H^+_{out} + k_{3b}H^+_{in};\ c^* \equiv -k_{2f}H^+_{out} + k_{3b}H^+_{in}$$

$$d \equiv k_{2b} + k_{3f};\ d^* \equiv k_{2b} - k_{3f}$$

$$e \equiv k_{4f}H^+_{out} + k_{5b}H^+_{in};\ e^* \equiv -k_{4f}H^+_{out} + k_{5b}H^+_{in}$$

$$f \equiv k_{4b} + k_{5f};\ f^* \equiv k_{4b} - k_{5f}$$

$$A \equiv aec + afc + adf + bdf$$

Following the previous analysis of Salom et al. [25], energetic barriers of unknown height and the energy wells of the histidine internal sites are taken to be spaced at fractional distances d_1, d_3, and d_2 respectively from the ground- to voltage-clamped side through the pore (Fig. 1).

Because the proton is charged, the rate constants will depend on the applied voltage. The dependence is calculated using the theory of absolute reaction rates from the voltage-dependent difference in barrier energies separating the two states involved in the specific rate process. For example, the rate constant governing transitions between the outside and the binding site is:

$$k_{0f} = k^o_{0f}\exp\left\{-\frac{eF}{RT}d_1V\right\} = k^o_{0f}\exp\left\{-\frac{d_1V}{25.7}\right\} \quad (2)$$

for voltage in mV units and 25°C [40]. Here, F is the Faraday constant, R the gas constant, and T the absolute temperature in K. If the voltage change is linear across the pore, the electrical distances correspond to geometrical distances, but this is not a necessary correspondence. Applying this analysis to the three-site model and assuming for simplicity a common set of barrier and site positions, the voltage-dependent rate constants become:

$$k_{nf} = k^o_{nf}\exp\{-d_1V/25.7\}$$

$$k_{nb} = k^o_{nb}\exp\{(d_2 - d_1)V/25.7\}$$

$$k_{(n+1)f} = k^o_{(n+1)f}\exp\{(d_2 - d_3)V/25.7\}$$

$$k_{(n+1)b} = k^o_{(n+1)b}\exp\{(1 - d_3)V/25.7\}$$

$$n = 0,\ 1,\ 2,\ 3,\ 4$$

Microscopic reversibility relates the forward and reverse rate constants for site protonation in the absence of the electrical field to the histidine site proton dissociation constants:

$$\frac{k^o_{0b}}{k^o_{0f}} = \frac{k^o_{0b}}{k^o_{0f}} = K_1;\ \frac{k^o_{2b}}{k^o_{2f}} = \frac{k^o_{3b}}{k^o_{3f}} = K_2;\ \frac{k^o_{4f}}{k^o_{4f}} = \frac{k^o_{5b}}{k^o_{5f}} = K_3$$

To further parameterize the model while maintaining thermodynamic consistency, the electrical distances were allowed to vary linearly with voltage, constraining their values to be-

[1] The f^* term arises from defining the S_3 site concentration as $1 - S_1 - S_2$ so its presence as an isolated constant term does not constitute a logical inconsistency; its contribution to currents is negligible in models considered here, where ks associated with site 3 are made negligibly small. However, these ks must be non-zero to compute current values. Results using the previously derived rigorous two-state model match those obtained with the 'disabled site' computation used here.

tween 0 and 1 while maintaining their defined relative positions. The validity of this procedure was confirmed by the accuracy and invariance of calculated reversal potentials to changes in the voltage dependence of the *d*s. In the final fittings, the rate constants for the 'in' side reactions (k_1,k_3,k_5) were allowed to differ by a constant factor from those for the 'out' side (k_0,k_2,k_4).

The current Eq. 1, together with the voltage dependent rate constants following the example of Eq. 2, was used with the least possible number of adjustable parameters necessary to acceptably fit selected data sets using the Levenberg–Marquardt algorithm of Igor Pro® (Wavemetrics, Oswego, OR, USA) with fitting weights derived from the published data error bars. For initial explorations, all of the 'on' rate constants (e.g. k_{0f}, k_{1b}) were taken to be equal (uniform diffusion-controlled protonation rate constants) and the electrical distances were assumed to be voltage-independent. For testing the simpler one- and two-state models, the rate constants corresponding to the unwanted higher protonation states were set to negligibly small values and the corresponding p*K*s set to negative values. Normalized (dimensionless), rimantidine-sensitive current versus pH and voltage data for both Weybridge and Rostock strain M2 protein (Table 1) expressed in MEL cells were extracted by graphical measurements from published figures [27].

3. Results

The first consideration in a quantitative analysis is that of the parameter magnitudes. They must have physically reasonable values and predict current magnitudes consistent with experimental data. In this model, current magnitude is determined primarily by the rates of histidine protonation and deprotonation. The maximum steady-state rate of His protonation can be roughly estimated from the diffusion-controlled limit using the Smoluchowski equation for flow from a hemispherical volume of radius r into a sink [40]:

$$\Phi_{\max} = 2\pi r D[\mathrm{H}^+]$$

where D is the diffusion coefficient for the proton and $[\mathrm{H}^+]$ the hydrogen ion concentration. Because the His is buried within the pore, the radius will be that of the pore, on the order of about 1 Å. With $D = 0.86$ Å^2/ps (its bulk value) and converted units, the expected on-rate constant for pH 6.0 will be about 3×10^9 1 site^{-1} s^{-1}. For a His p$K_a = 6.0$, the corresponding off-rate per site would be 3×10^3 s^{-1}. However, the transport of protons in such a narrow pore can be heavily influenced by structural details. At one extreme, proton diffusion has been calculated to occur at a rate 10 times its bulk value for the special case of a uniformly cylindrical 2 Å radius pore [41]. At the other extreme, interruption of water connectivity [4] or rotational immobilization of side chains [38] can essentially stop this type of proton transport.

Table 1
Partial sequences including the putative transmembrane segment of Weybridge and Rostock M2 and data sets used in data fitting

Set	pH_{in}	pH_{out}	Voltage (mV)	Source [27] figure
1	7	7 to 3	0	1
2	7	7 to 3	−60	1
3	7	5	−80 to +80	2
4	8	6	−80 to +80	6
5	6	8	−80 to +80	6

Sets 1 and 2 are for Rostock only. Sets 3, 4, and 5 include data from both strains.

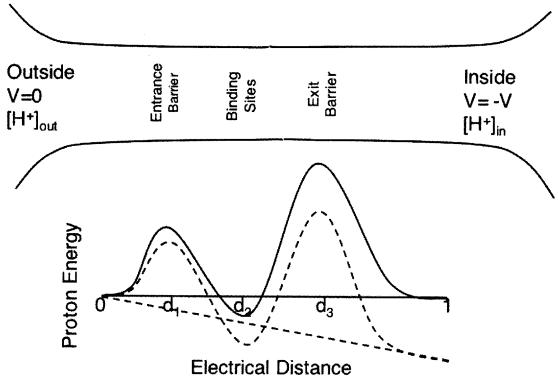

Fig. 1. Diagrammatic representation of the proton channel (top) and proton energy profiles (bottom) for one of the sites at zero (solid) and V (dashed) applied voltage. The inside and outside reservoirs are each maintained at constant pH and the voltage zero (ground) is on the outside.

The influence of the pore interior on the His pK_a is not known in detail. A survey of His-containing proteins of known structure shows an average buried His pK_a of 6.6 ± 1 but individual pK_as range between <3 and 9, depending on the local environment [42]. With four His residues confined to the same interior location, it seems reasonable to expect significant negative cooperativity in successive protonations. The study of Salom et al. [25] suggested a first pK_a of $\sim$6.5 and a second of 5.7 or less.

The electrical current per channel is obtained by converting moles of protons per second per site into amperes (coulombs/s) using the Faraday constant (96 500 C/mol). The single-channel conductance, defined as the derivative of current with respect to voltage, can be computed from the current–voltage curve. Because current–voltage curves are significantly non-linear, it is useful to define the conductance as the slope of the I–V curve near the zero-current voltage. At this condition, we compute a maximum single-channel conductance at pH 6.0 of about 15 fS, reasonably consistent with earlier upper limit estimates [28]. Reported experimental values are all much lower than this [23,33], suggesting, not surprisingly, that proton diffusion is slower in the pore than it would be in bulk water. This is an important point to be discussed later.

The voltage- and pH-dependences of the currents are, of course, the key tests of any proposed mechanism. Data set 1, having been measured using a pH pulse protocol with no transmembrane voltage gradient, afforded an opportunity to test the mechanism free from any influence from the electrical distance parameters. Applying the current Eq. 1 (normalized using reference conditions appropriate to each set), we found that equally satisfactory data fits (see Fig. 2, inset) could be obtained with a single p$K_1 = 5.4\pm0.2$, with 2 p*K*s (p$K_1 >$ pK_2, p$K_2 = 5.4\pm0.2$), and with three pK_as (pK_1, p$K_2 >$ pK_3, p$K_3 = 5.4\pm0.2$). Fits with two or three identical p*K*s (not shown) were unsatisfactory (excessively cooperative). As pointed out by Chizhmakov et al. [27], the data can also be fit by a single site binding function with a pK of 5.09. This pK is slightly, but significantly smaller than the His pK needed to fit the data with the more appropriate current equation, showing the advantage of the more rigorous analysis.

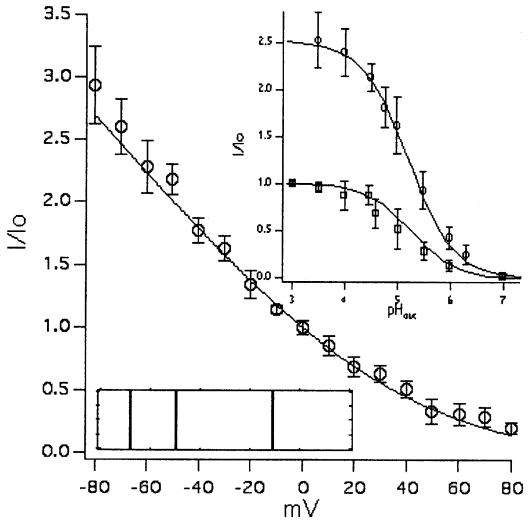

Fig. 2. Global fit (lines) of Rostock strain data (points) from sets 1, 2, (upper right inset) and 3 (I/I_0 versus mV). Inset at lower left shows fitted values of the electrical distance parameters. Inset x-axis ranges from 0 to 1. The y-axis is voltage ranging over ±80 mV. For these fits, a single site model with $pK_1 = 5.55$ was assumed and electrical distances were independent of voltage. Current ratios were calculated as in [27] except the sign was maintained positive for mathematical consistency.

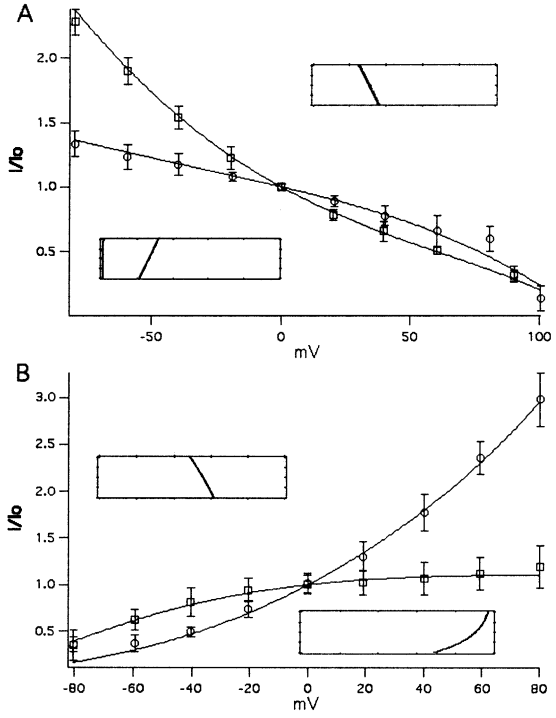

Fig. 3. Single fits (lines) of inward (A) and outward (B) currents from sets 3 and 4 including both Rostock (circles) and Weybridge (squares) strain data. For these fits, a single-site model with $pK_1 = 5.55$ (Rostock) or $pK_1 = 5.7$ (Weybridge) was assumed. Insets (A, upper-Weybridge, lower-Rostock; B, upper-Rostock, lower-Weybridge) in both panels show fitted values of the electrical distance parameters plotted as in Fig. 2.

A far more sensitive test of any conduction mechanism is its ability to account for both voltage- and pH-gradient changes. Thus, data sets 1, 2, and 3 were selected for simultaneous fitting with a common set of parameters. Fig. 2 shows that acceptable fits to pH dependences at both 0 and −60 mV, and to inward currents measured from −80 to +80 mV with $pH_{out} = 6.0$, $pH_{in} = 5.0$ can be obtained with a slightly higher, single pK (5.55) and with barrier and site positions shown in the inset. It is important to note that the positions do not necessarily correspond to geometric distances in the pore. For example, a large vestibule at the channel entrance would tend to shift the applied voltage gradient toward the channel exit. In effect, the channel structure defines the relationship between electrical and geometric distances so the latter are a potentially useful probe of structural changes.

To further probe the model, attempts were made to globally fit all Rostock strain data sets, including current–voltage curves for $pH_{out} = 6.0$, $pH_{in} = 8.0$ and the reverse pH gradient (sets 4 and 5). This was unsuccessful despite many attempts using more protonation states, an additional proton-selective current not involving His, and allowing voltage-dependent changes in barrier and site positions. Restricting data analysis to sets 4 and 5 was equally unsuccessful. Instead, fits could only be obtained for individual sets, each of which had a unique pH gradient and a unique set of barrier and site positions. Fits and corresponding voltage-dependent barrier and site positions for data sets 4 and 5 are shown in Fig. 3. Such large changes in the locations of the site and barrier positions seem unlikely, but are not impossible if there were large, pH-dependent changes in the electrical environment within the channel. Whatever the underlying cause, it seems clear from this analysis that changes beyond His protonation must be occurring with changes of pH in the M2 channel.

All of the above analysis was done under the assumption of a common, diffusion-controlled rate of histidine protonation. This is not, however, a necessary assumption. It is quite conceivable that proton diffusion rates from the inside and from the outside differ due to differences in water–wire connectivity and/or rotational freedom of proton donor/acceptors. Such a situation, involving Trp[41] side-chain interference with the proton pathway, has, in fact, been postulated to explain the low outward currents and internal inaccessibility of the His bind-

Table 2
Summary of fit parameters determined for data shown in Fig. 4

Strain	pH_{out}	pH_{in}	pK_2	Out barrier (d_1)	Sites (d_2)	In barrier (d_3)	Log (D_{in}/D_{out})
Rostock	3	7	5.55	0.09	0.27	0.66	0 ± 1
Rostock	5	7	5.55	0.09	0.27	0.66	< −0.5
Rostock	6	8	5.55	0.09	0.27	0.66	> 2
Rostock	8	6	5.55	0.09	0.27	0.66	−2.8 ± 0.2
Weybridge	4	7.5	5.67	0.24	0.64	0.92	0 ± 0.5
Weybridge	5	7	5.67	0.24	0.64	0.92	0 ± 5
Weybridge	6	8	5.67	0.24	0.64	0.92	> 1.5
Weybridge	8	6	5.67	0.24	0.64	0.92	−1.5 ± 0.2

pK_1 was 6.5 in all cases.

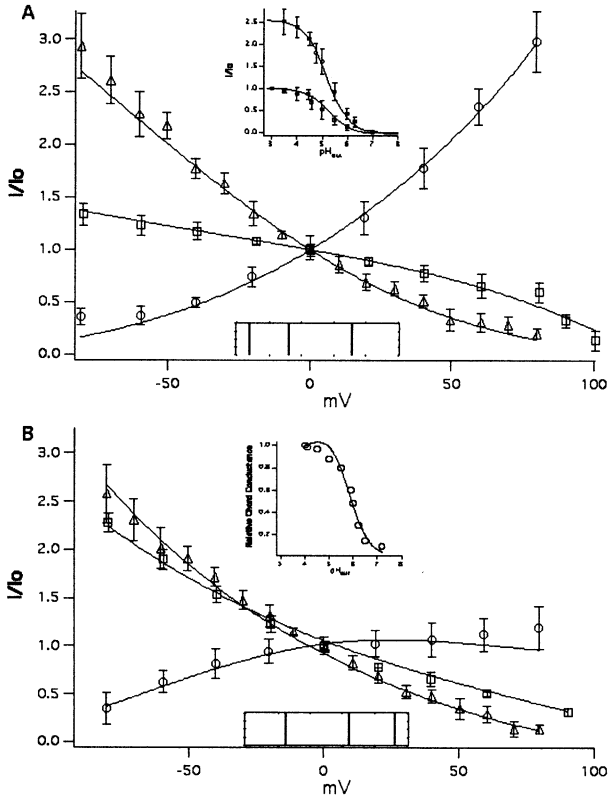

Fig. 4. A: Global fit (lines) of Rostock strain data (points) from sets 1 and 2 (upper inset), and from sets 3 (triangles), 4 (circles), and 5 (squares). B: Global fit (lines) of Weybridge strain data (points) from previously analyzed [25] Weybridge chord conductance–pH data [26] and from sets 3, 4, and 5 as in panel A. For these fits, a two-site model was employed using $pK_1 = 6.5$ and $pK_2 = 5.55$ (Rostock) or 5.67 (Weybridge). Electrical distance parameters were common for each strain and voltage-independent for all data sets, but diffusional asymmetry allowed to vary individually for each set. Lower insets show fitted values of the electrical distance parameters as in Fig. 2. Fit parameters are shown in Table 2.

ing site at high external pH [34]. It is important to note here that microscopic reversibility requires that the site p*K*s not be affected by diffusional asymmetry. The p*K*s are determined by the site 'well' energies relative to the baths. Raising or lowering the barriers affects on- and off-rates equally, leaving p*K* invariant. While direct computation (not shown) shows that absolute currents are proportionally reduced with reduced inner (and/or outer) diffusion coefficients, there is surprisingly little effect of diffusional asymmetry alone on the ratio of inner and outer currents. Only when the asymmetry is made to depend on pH do dramatic effects appear.

To probe the possible effects of pH-dependent diffusional asymmetry, the 'in' side rate constants were multiplied by a constant and this constant, interpretable as the ratio of inside to outside diffusion constants, was allowed to differ for the different pH gradients in all of the data sets. In addition, although not necessary for fitting, a two-site model was employed using a first pK_a of 6.5 to show consistency with earlier estimates of this value [25]. Re-fitting of all these data together, now with global and voltage-independent electrical distance parameters, was successful (Fig. 4A). Current–voltage data for the Weybridge strain at the same pH gradients as sets 4 and 5 could similarly be fit (Fig. 4B) with only slightly different values for the parameters (Table 2).

The log D_{in}/D_{out} ratios necessary for the fit varied with pH in an interesting manner; at low pH_{out}, (represented by the pH-dependent data of sets 1 and 2) the log of the ratio was 0 ± 1 (errors estimated by visually comparing fits for the stated range of values). At the two intermediate pH_{out}s, (pH 5 and 6) the log ratio increased to 2 ± 1 and > 2, respectively. Finally, at $pH_{out} = 8$, the log ratio falls sharply to -2.8 ± 0.2, a behavior consistent with previously reported pH gating [34]. A similar trend is observed for the Weybridge strain. This complex behavior could in principle arise from a process of pH gating of both in and out side pore regions, where each region has a slightly different pH response. If one looks instead at the dependence of these ratios on pH_{in}, the ratio decreases steadily with internal pH, again indicative of a gating process, but one different from that previously postulated for the Trp-dependent gating process [34]. It is impossible to determine which is the more relevant dependence from these data.

Absolute values of M2 currents calculated using the upper limit k^os and global fit parameters determined for the data in Fig. 2 and with no diffusional asymmetry are over an order of magnitude larger than those measured previously [23,33]. Structural impediments to pore proton diffusion could account for the lower-than-maximum currents. Other possible causes include low partitioning of protons from the bulk into the channel (although this does not appear to be a factor for the gramicidin channel [43]), and a low intrinsic probability for channels to be open [28,33]. What is important is that the magnitudes of all measured M2 currents are well within the limits expected for the site-binding model considered here and at least qualitatively consistent with the diffusional limitations we found necessary for data fitting.

4. Discussion

This work shows that M2's proton conduction properties can be quantitatively explained by a model involving conventional protonation equilibria of His^{37} along with pH-dependent changes in the relative rates of diffusion on either side of the pore. The pH dependences of the currents indicate that the four histidines forming the proton binding sites are protonated successively rather than simultaneously with decreasing pH. Differences between Rostock and Weybridge strains can be related primarily to a relatively small shift in the electrical environment around His^{37}. Interestingly, the shift appears to be associated in part with a change in N^{44} (Rostock) to D^{44} (Weybridge), which might reasonably be expected from the helical periodicity to affect the electrical potential within the pore. The pH dependence of relative diffusion rates inferred from this work is consistent with earlier work indicating an important role of Trp^{41} in pH gating, but the limited data considered here cannot establish what this role might be nor how pH affects it. Rates involving His^{37} protonation equilibrium clearly dominate the conduction process; other processes which by-pass this process, such as H_3O^+ flux in a widened pore [10,12,37] or substitution of His for water in the 'water–wire' mechanism suggested by molecular dynamics simulations [38], fail to account for current saturation near pH 3. We hope this work will stimulate systematic experimental investigations designed to further test the suggested mechanism and, perhaps, use its parameters together with structural models to relate sequence changes to associated changes in conductance properties.

Acknowledgements: This work was supported by NIH Grant GM-54623. Thanks to William DeGrado and Lawrence Pinto for many helpful discussions and constructive comments.

References

[1] Brzezinski, P. (2000) Biochim. Biophys. Acta 1458, 148–163.
[2] Page, C.C., Moser, C.C., Chen, X. and Dutton, P.L. (1999) Nature 402, 47–52.
[3] Nagle, J.F. and Morowitz, H.J. (1978) Proc. Natl. Acad. Sci. USA 75, 298–302.
[4] Brandsburg-Zabary, S., Fried, O., Marantz, Y., Nachliel, E. and Gutman, M. (2000) Biochim. Biophys. Acta 1458, 120–134.
[5] DeCoursey, T.E. and Cherny, V.V. (2000) Biochim. Biophys. Acta 1458, 104–119.
[6] Lamb, R.A., Holsinger, L.J. and Pinto, L.H. (1994) in: Receptor-Mediated Virus Entry into Cells (Wimmer, E., Ed.), pp. 303–321, Cold Spring Harbor Press, Cold Spring Harbor, NY.
[7] Pinto, L.H. et al. (1997) Proc. Natl. Acad. Sci. USA 94, 111301–111306.
[8] Zhong, Q., Husslein, T., Moore, P.B., Newns, D.M., Pattnaik, P. and Klein, M.L. (1998) FEBS Lett. 434, 265–271.
[9] Zhong, Q., Newns, D.M., Pattnaik, P., Lear, J.D. and Klein, M.L. (2000) FEBS Lett. 473, 195–198.
[10] Forrest, L.R., Kukol, A., Arkin, I.T., Tieleman, D.P. and Sansom, M.S. (2000) Biophys. J. 78, 55–69.
[11] Kerr, I.D., Sankararamakrishnan, R., Smart, O. and Sansom, M. (1994) Biophys. J. 67, 1501–1515.
[12] Sansom, M.S.P., Kerr, I.D., Smith, G.R. and Son, H.S. (1997) Virology 233, 163–173.
[13] Torres, J., Kukol, A. and Arkin, I.T. (2000) Biophys. J. 79, 3139–3143.
[14] Kovacs, F.A. and Cross, T.A. (1997) Biophys. J. 73, 2511–2517.
[15] Bauer, C.M., Pinto, L.H., Cross, T.A. and Lamb, R.A. (1999) Virology 254, 196–209.
[16] Nishimura, K., Kim, S., Zhang, L. and Cross, T.A. (2002) Biochemistry 41, 13170–13177.
[17] Song, Z., Kovacs, F.A., Wang, J., Denny, J.K., Shekar, S.C., Quine, J.R. and Cross, T.A. (2000) Biophys. J. 79, 767–775.
[18] Wang, J., Kim, S., Kovacs, F. and Cross, T.A. (2001) Protein Sci. 10, 2241–2250.
[19] Sakaguchi, T., Tu, Q., Pinto, L.H. and Lamb, R.A. (1997) Proc. Natl. Acad. Sci. USA 94, 5000–5005.
[20] Wang, C., Lamb, R.A. and Pinto, L.H. (1995) Biophys. J. 69, 1363–1371.
[21] Gandhi, C.S., Shuck, K., Lear, J.D., Dieckmann, G.R., DeGrado, W.F., Lamb, R.A. and Pinto, L.H. (1999) J. Biol. Chem. 274, 5474–5482.
[22] Hay, A.J., Wolstenholme, A.J., Skehel, J.J. and Smith, M.H. (1985) EMBO J. 4, 3021–3024.
[23] Holsinger, L.J., Nichani, D., Pinto, L.H. and Lamb, R.A. (1994) J. Virol. 68, 1551–1563.
[24] Hay, A.J. (1992) Sem. Virol. 3, 21–30.
[25] Salom, D., Hill, B.R., Lear, J.D. and DeGrado, W.F. (2000) Biochemistry 39, 14160–14170.
[26] Chizhmakov, I.V., Geraghty, F.M., Ogden, D.C., Hayhurst, A., Antoniou, M. and Hay, A.J. (1996) J. Physiol. 494, 329–336.
[27] Chizhmakov, I.V., Ogden, D.C., Geraghty, F.M., Hayhurst, A., Skinner, A., Betakova, T. and Hay, A.J. (2003) J. Physiol. 546, 427–438.
[28] Mould, J.A., Li, H.C., Dudlak, C.S., Lear, J.D., Pekosz, A., Lamb, R.A. and Pinto, L.H. (2000) J. Biol. Chem. 275, 8592–8599.
[29] Pinto, L.H., Holsinger, L.J. and Lamb, R.A. (1992) Cell 69, 517–528.
[30] Shimbo, K., Brassard, D.L., Lamb, R.A. and Pinto, L.H. (1996) Biophys. J. 70, 1336–1346.
[31] Wang, C., Takeuchi, K., Pinto, L.H. and Lamb, R.A. (1993) J. Virol. 67, 5585–5594.
[32] Wang, C., Lamb, R.A. and Pinto, L.H. (1994) Virology 205, 133–140.
[33] Lin, T.I. and Schroeder, C. (2001) J. Virol. 75, 3647–3656.
[34] Tang, Y., Zaitseva, F., Lamb, R.A. and Pinto, L.H. (2002) J. Biol. Chem. 277, 39880–39886.
[35] Duff, K.C. and Ashley, R.H. (1992) Virology 190, 485–489.
[36] Schweighofer, K.J. and Pohorille, A. (2000) Biophys. J. 78, 150–163.
[37] Kukol, A. and Arkin, I.T. (2000) J. Biol. Chem. 275, 4225–4229.
[38] Smondyrev, A.M. and Voth, G.A. (2002) Biophys. J. 83, 1987–1996.
[39] Kienker, P.K. and Lear, J.D. (1995) Biophys. J. 68, 1347–1358.
[40] Hille, B. (1992) Sinauer Associates, Inc., Sunderland, MA.
[41] Brewer, M.L., Schmitt, U.W. and Voth, G.A. (2001) Biophys. J. 80, 1691–1702.
[42] Edgcomb, S.P. and Murphy, K.P. (2002) Proteins 49, 1–6.
[43] DeCoursey, T.E. and Cherny, V.V. (1994) J. Gen. Physiol. 103, 755–785.